Supporting Information for

Atomic-layer precision etching of SiO2 using sequential molecular adsorption and plasma activation

Rakshith Venugopal[1], Nian Ran[2]*, Robert Blick[1,3], Robert Zierold[1]*, Jun Peng[1]*.

1 Center for Hybrid Nanostructures, University of Hamburg, Luruper Chaussee 149, 22607 Hamburg, Germany

2 State Key Laboratory of High-Performance Ceramics and Superfine Microstructures, Shanghai Institute of Ceramics, Chinese Academy of Sciences, 200050 Shanghai, China

3 DESY Photon Science Deutsches Elektronen-Synchrotron DESY, 22607 Hamburg, Germany

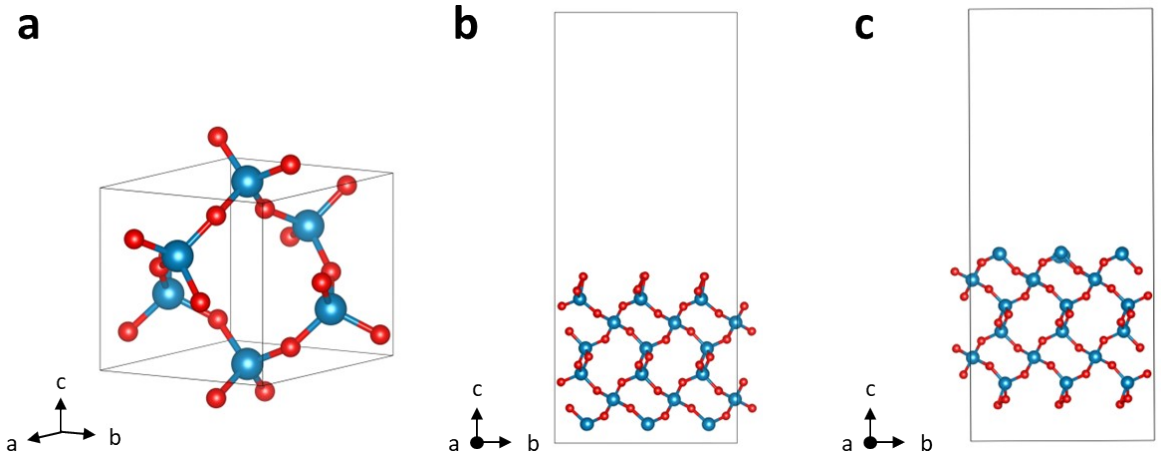

Figure S1. DFT models. (a) SiO_2 unit cells. The initial SiO_2 structure (α-quartz, space group $P3_221$, No. 154) was constructed with lattice parameters $a = b = 4.91656$ Å, $c = 5.43163$ Å. Subsequent DFT relaxation yielded equilibrium lattice parameters of $a = b = 5.03$ Å and $c = 5.51$ Å, deviating by less than 2.31% from experimental values, confirming good consistency. Based on the optimized bulk structure, a SiO_2 (001) surface slab was built using a 2×2×2 supercell of the conventional unit cell, comprising 162 atoms in total. A 20 Å vacuum slab was introduced along the z-direction to avoid spurious interactions between periodic images. (b) O-terminated and (c) Si-terminated 2×2×2 supercells were constructed for adsorption calculations. In these slab models, the top three atomic layers, presenting the reactive surface and sub-surface regions, were allowed to relax fully until the forces met the convergence criterion, whereas the bottom three layers were fixed at their optimized bulk positions to mimic the bulk environment and prevent artificial slab relaxations. For geometry optimizations of both clean and adsorbate-covered surfaces, Brillouin zone sampling was performed using a 2 × 2 × 1 Monkhorst–Pack *k*-point grid. In all surface and adsorption calculations, the lattice constants were fixed to the pre-optimized bulk values (ISIF = 2 in VASP), as it is physically reasonable to constrain the substrate lattice during surface reactions.

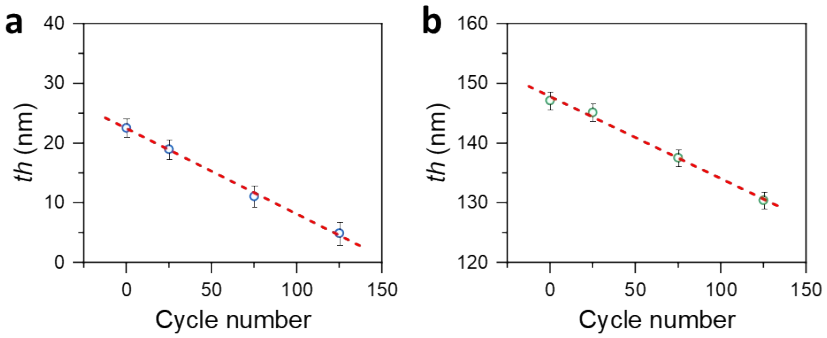

Figure S2. SiO_2 thickness variation as a function of etching cycles for comparative samples using the standard recipe. (a) The EPC resulting from etching 22.55 nm ALD-deposited SiO_2 is 1.43 Å/cycle. (b) The EPC resulting from etching 147.15 nm ALD-deposited SiO_2 is 1.37 Å/cycle. Both values are comparable to the EPC of 1.41 Å/cycle obtained by etching thermally oxidized SiO_2. This indicates that the etching process is governed by surface reaction kinetics rather than bulk material properties or the processing history of SiO_2 material.

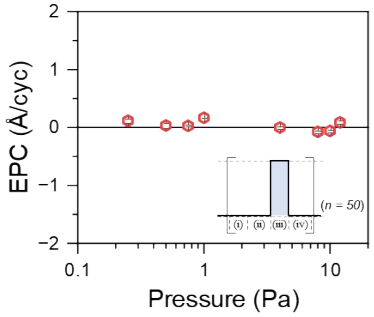

Figure S3. EPC as a function of etching pressure. In this control experiment, step (i) SF_6 exposure in the standard recipe is replaced with a blank period, and the chamber pressure is varied. The EPC remains zero across the tested pressure range, indicating that Ar plasma alone does not induce sputtering-based etching of SiO_2 under these conditions.

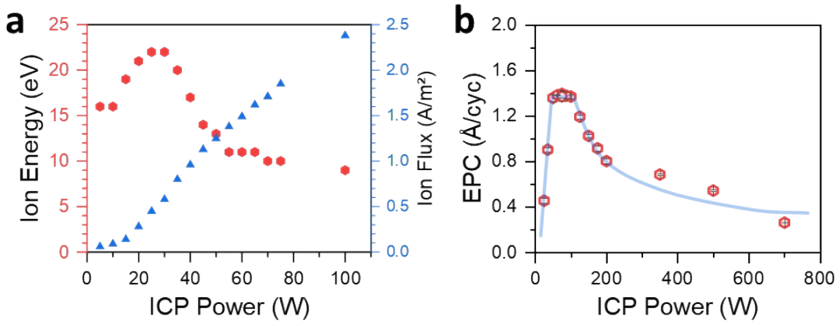

Figure S4. EPC and ion characteristics as a function of ICP power at 1 Pa. (a) Ion energy and ion flux versus ICP power, measured using the same ICP-RIE system model (data provided by SENTECH Instruments GmbH). At low ICP powers, the plasma operates in the electrostatic (E-mode) regime, similar to normal capacitively coupled plasma (CCP) that are characterized by low plasma density, high electron temperature, and moderate ion energy. As power increases, ion energy peaks around 30 W due to optimal sheath potential and moderate collisional damping. Further increasing in ICP power leads to higher plasma density, lower electron temperature, reduced sheath potential, and increased collisional losses, causing a decline in ion energy. In this regime, the plasma transitions to inductively coupled (H-mode), where electromagnetic driving dominates and capacitive coupling diminishes. (b) EPC as a function of ICP power. The overall shape of the EPC curve mirrors the trend in ion energy, suggesting that the EPC curve is influenced by the E-mode to H-mode transition. The expansion and shift of the EPC curve toward higher powers can be attributed to operating at lower gas pressure, which increases the E–H mode transition threshold by limiting ionization efficiency. While factors such as gas composition, chamber geometry, and coil design also affect the transition point, these variables can be considered as constant in this analysis due to measurements being performed on the same equipment model.

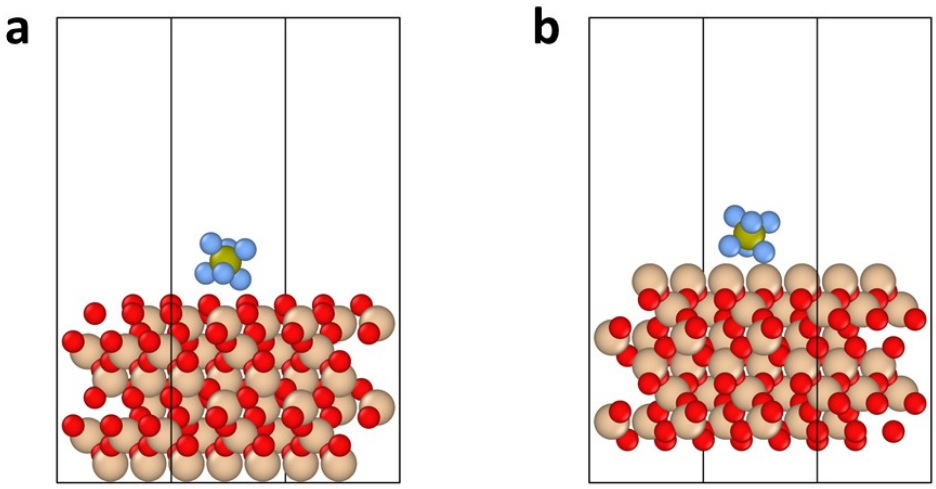

Figure S5. AIMD simulations were conducted to evaluate the interaction between SF_6 molecules and SiO_2 surfaces terminated by (a) O atoms and (b) Si atoms. As shown in video S1 and video S2 corresponding to (a) and (b), SF_6 molecules do not react with the O-terminated surface, whereas the Si-terminated surface facilitates chemical adsorption of F atoms dissociated from SF_6 molecules.

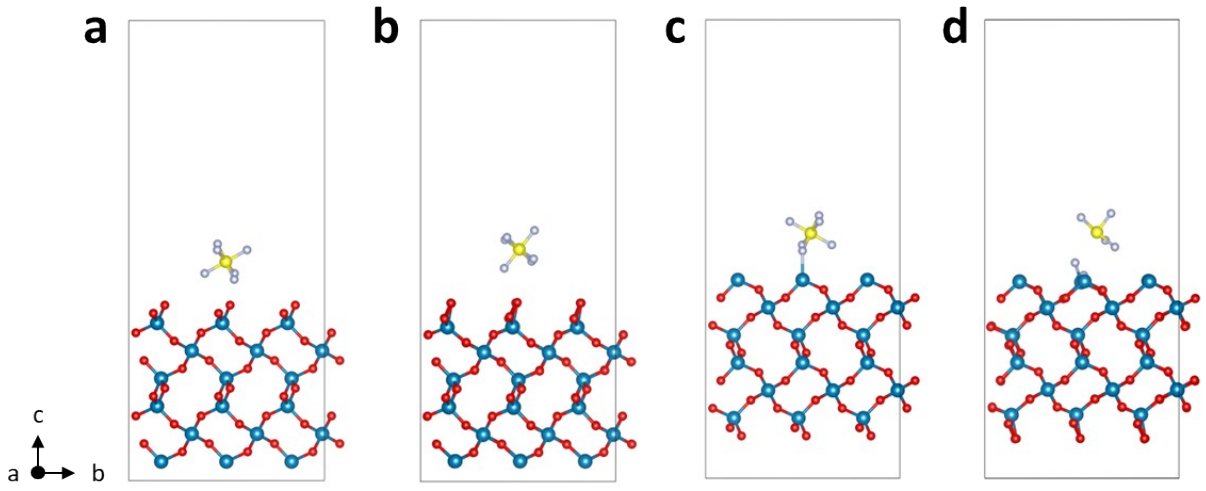

Figure S6. DFT-calculated adsorption behavior of SF_6 molecules on SiO_2 surfaces with different terminations. (a,b) O-terminated SiO_2 surface before and after relaxation. The calculated adsorption energy E_{ads} is -0.22 eV, and no chemisorption phenomena has been found. (c,d) Si-terminated SiO_2 surface before and after relaxation. F atoms dissociate from SF_6 and bond to surface Si atoms, with an adsorption energy E_{ads} of –5.98 eV, confirming strong chemisorption. Adsorption energies were calculated as $E_{ads} = E_{slab+SF_6} - E_{slab} - E_{SF_6(gas)}$, where $E_{slab+SF_6}$, E_{slab}, and $E_{SF_6(gas)}$ represent the total energies of the adsorbed system, the pristine SiO_2 slab, and the isolated SF_6 molecule, respectively. These results reveal that SF_6 preferentially chemisorbs on Si-terminated surface defects, consistent with the AIMD calculation results.

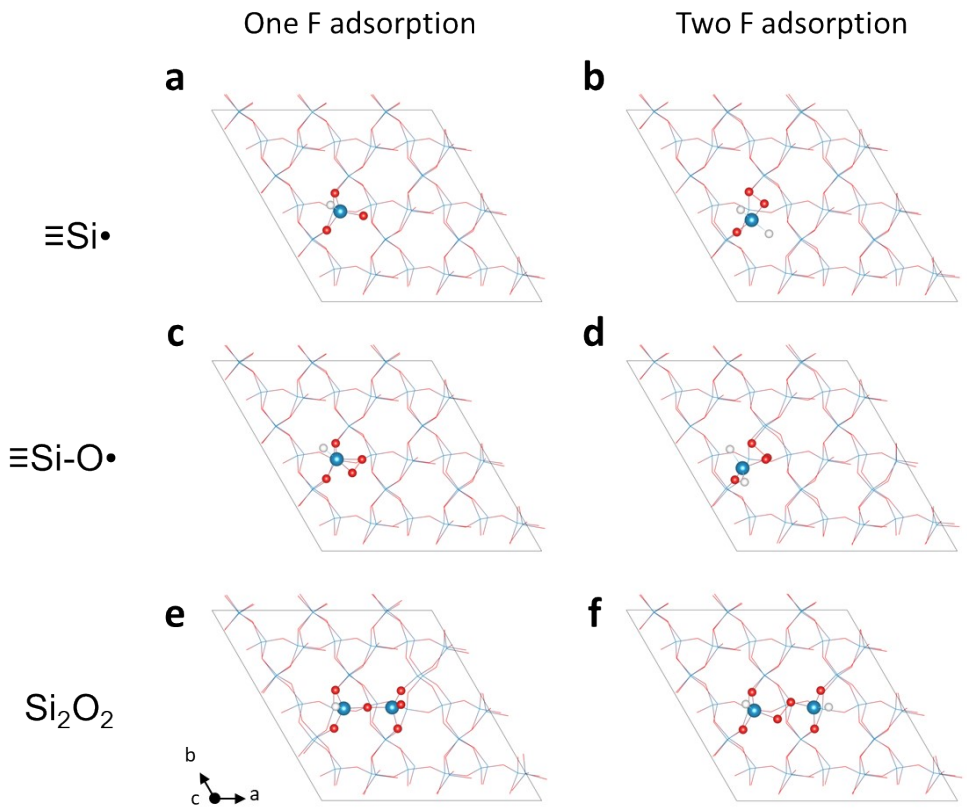

Figure S7. Adsorption configurations of F atoms at SiO_2 surface defects. DFT-optimized structures showing the adsorption of one (left) or two (right) F atoms at representative defect sites on the SiO_2 surface: (a, b) silicon dangling bond (≡Si•), (c, d) oxygen-centered radical (≡Si–O•), and (e, f) strained Si_2O_2 ring. These configurations illustrate the local bonding environment and stability of F adsorption at each defect type.

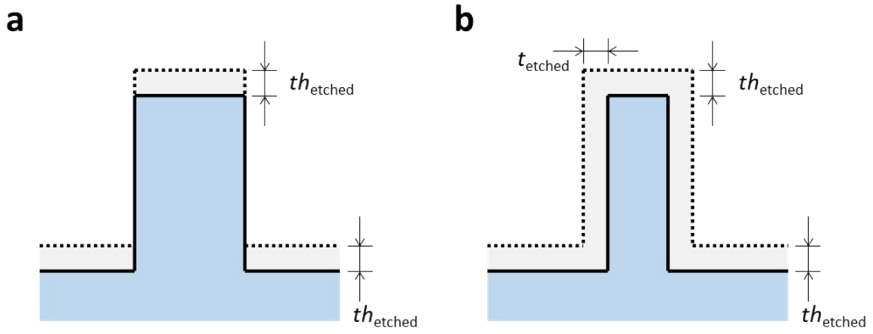

Figure S8. Comparison of directional etching and isotropic etching. (a) Directional etching will only etch in the vertical direction, not in the horizontal direction. (b) However, in isotropic etching, the cylinder will be uniformly etched in both the vertical and horizontal directions, resulting in a reduction in diameter.

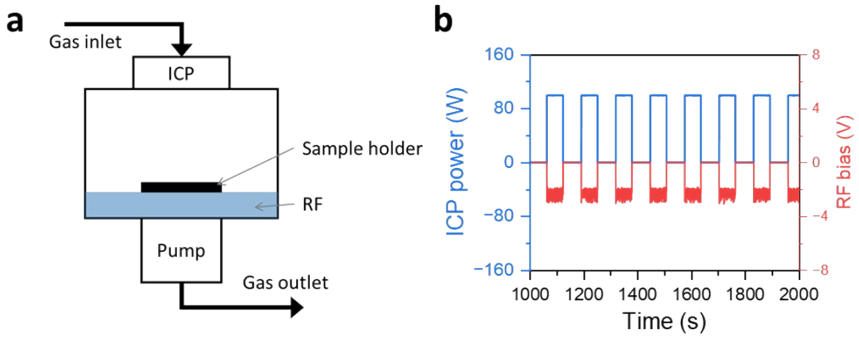

Figure S9. Indirect bias voltage. (a) The sketch of the reactor. (b) Part of the instrument log showing the detected ICP power and RF power during the experiment. During the experiment, only the ICP on the top of the sample was activated in the form of pulses, and the RF power was set to zero. Every time the ICP was activated, a passively generated RF bias was recorded. This bias will make the plasma directional.

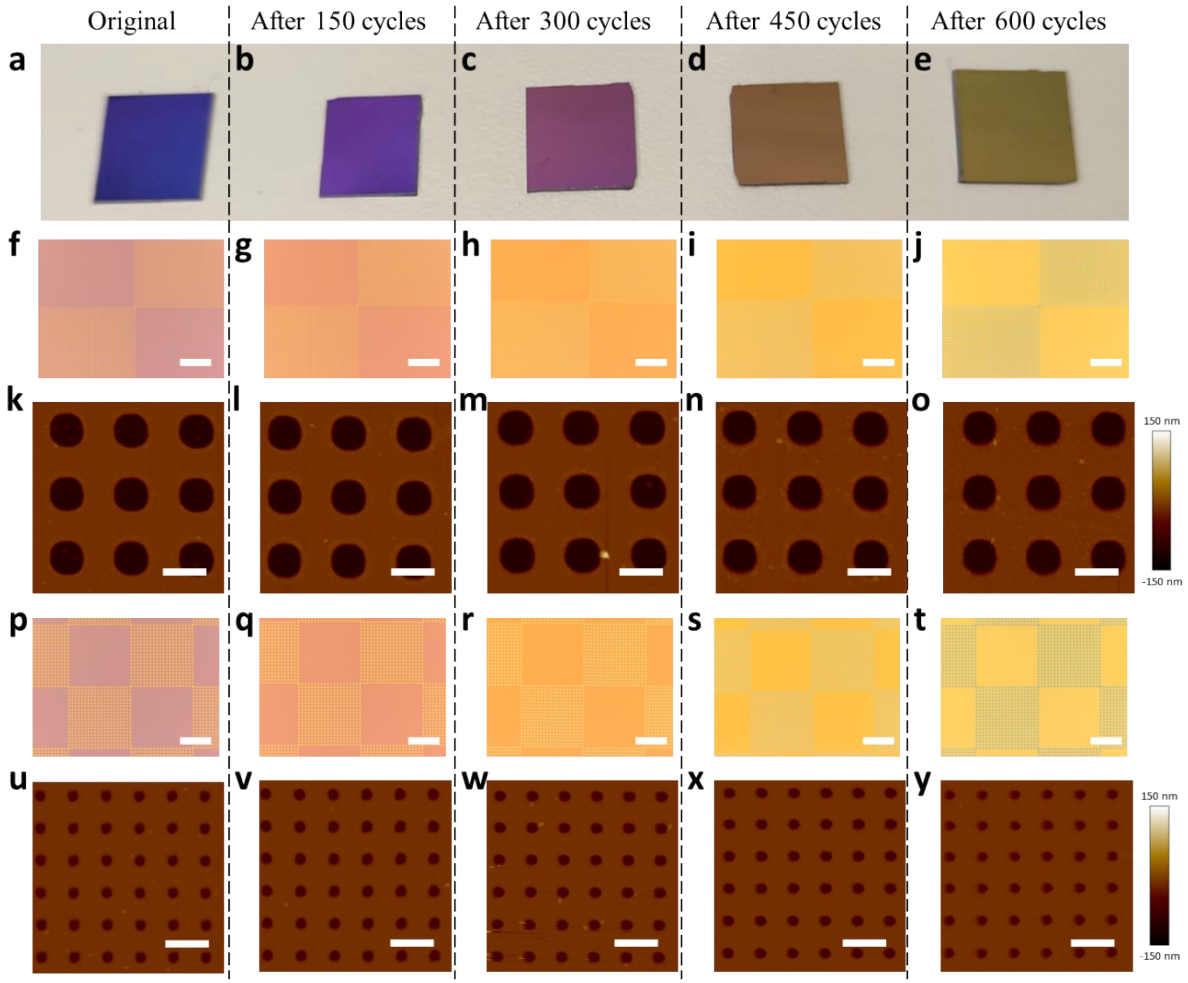

Figure S10. Holes sample for the etching effect test. (a~e) Photo of the etching reference samples. The size of the five reference samples is about 1 cm × 1 cm. Samples (b)~(e) were placed in the reaction chamber at the first batch and taken out after the corresponding etching batch in turns. (f~j) Optical images of the same sample, with a hole diameter of about 1.2 μm, at the same position after different number of etching cycles. (k~o) AFM images of the same sample after different number of etching cycles corresponding to the sample in (f~j). (p~t) Optical images of the same sample, with a hole diameter of about 0.6 μm, at the same position after different number of etching cycles. (u~y) AFM images of the same sample after different number of etching cycles corresponding to the sample in (p~t). Etching reduces the thickness of the SiO_2 film, causing the color of the film to change, but the diameter of the pores does not change. The scalebar for (f~j), (k~o), (p~t), and (u~yt) are 20 μm, 2 μm, 20 μm, and 2 μm.

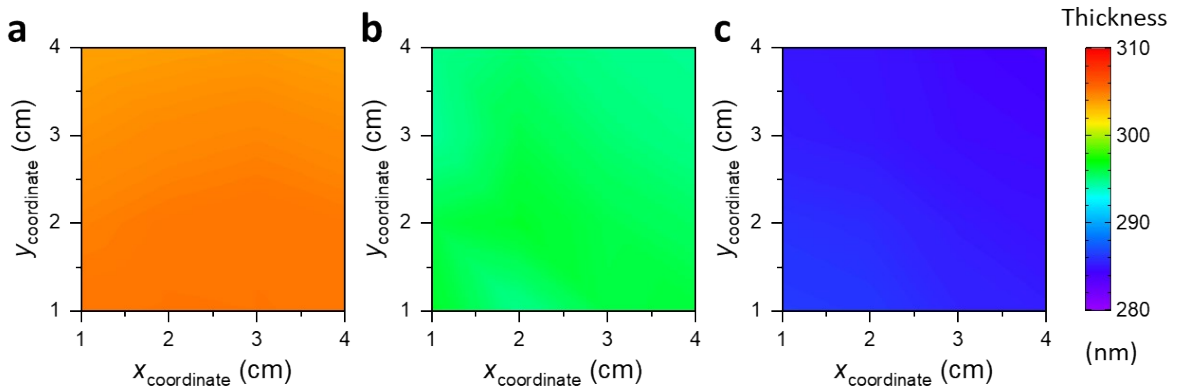

Figure S11. Uniformity test on the same SiO_2/Si wafer with a 4.5 cm × 4.5 cm size. (a) The thickness of the SiO_2 layer of the original sample is 304.7 ± 0.54 nm. (b) The thickness of the SiO_2 layer after 75 cycles is 295.5 ± 0.67 nm, and 9.2 ± 0.51 nm is etched. (c) The thickness after another 75 cycles, in total of 150 cycles, is 285.2 ± 0.61 nm, and 19.5 ± 0.50 nm is etched. The test was performed at a 4 cm × 4 cm area with a spacing of 1 cm. Each measurement was made at the same location. The standard deviations of the etched thickness after 75 cycles and 150 cycles are all around 0.5 nm, indicating good intra-wafer uniformity of the etching. The etch uniformity, $Uniformity\ (\%) = \frac{thickness\max\ -\ thickness\ min}{2\ \times average\ thickness\ removed} \times 100\%$, for the first 75 cycles etching is 10.3%, for the total 150 cycles is 3.96%.

Table S1. EPC comparisons of reported SiO2 etching using ALE manner.

Time	Reactant A	Reactant B	Further reactants	EPC (Å/cyc)	ref
2017-02	Trimethylaluminum ($Al(CH_3)_3$)	HF	--	0.027 (0.1 Torr) 0.15 (0.5 Torr) 0.2 (1 Torr) 0.31 (4 Torr)	17
2017-05	C_4F_8 plasma	Ar plasma	--	1.9	31
2017-08	C_4F_8/Ar plasma	Ar plasma	--	3 ~ 4	32
2017-12	CHF_3 plasma	O_2 or Ar plasma	--	6.8 (O_2 plasma) 4.0 (Ar plasma)	33
2019-05	Ar plasma	CHF_3	--	10.7	34
2019-08	C_4F_8/Ar plasma	Ar plasma	--	2.6	41
2019-09	CHF_3	Ar Plasma	--	10 ~ 15	35
2021-08	CHF_3/O_2 plasma	infrared annealing		2.5	19
2021-10	HF	NH_3	infrared annealing	9.09	42
2021-10	H_2, SF_6 plasma	NH_3	infrared annealing	27.0	42
2022-07	CF_3I plasma	O_2 plasma	--	9.8	36
2022-07	C_4F_8	Ar Plasma	--	20	37
2023-04	Heptafluoropropyl methyl ether (HFE-347mcc3)	Ar plasma	--	2.1	38
2023-04	Heptafluoroispropyl methyl ether (HFE-347mmy)	Ar plasma	--	1.8	38
2023-04	Perfluoro propyl carbinol (PPC)	Ar plasma	--	5.2	38
2023-12	SF_6 plasma	Ar plasma	--	2.3 (without bias) 5 (with bias)	39
2024-01	C_4F_8	Ar plasma	--	5.5	40
2024-01	perfluoroisopropyl vinyl ether (PIPVE)	Ar plasma	--	3.3	40
2024-01	perfluoropropyl vinyl ether (PPVE)	Ar plasma	--	5.4	40
2024-05	Trimethylaluminum ($Al(CH_3)_3$)	$Ar/H_2/SF_6$ plasma	--	0.52 (SiO_2) 0.78 (ALD SiO_2) 1.52 (PECVD) 2.38 (Sputtered)	18
★	SF_6	Ar plasma	--	1.4	This work

Table S2. Comparison of different etching mechanisms.

#	Schematic	Parameters	EPC (Å/cyc)
2-1*	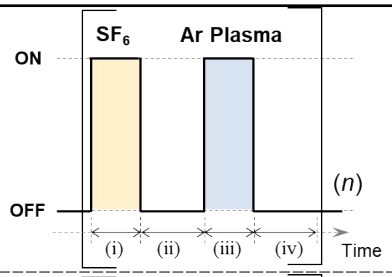	(i) SF_6, 20 sccm: 10 s (ii) Purge: 30 s (iii) Ar, 100 sccm: 100 W, 60 s (iv) Purge: 30 s Cycle number n = 50	1.38 ± 0.03
2-2	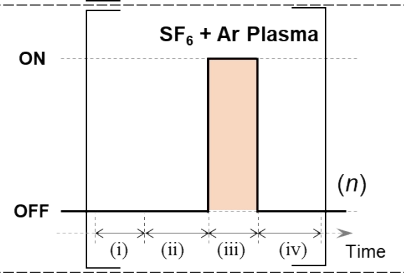	(i) Wait for 10 s (ii) Purge: 30 s (iii) SF_6, 20 sccm + Ar, 100 sccm: 100 W, 60 s (iv) Purge: 30 s Cycle number n = 50	31.27 ± 0.02
2-3	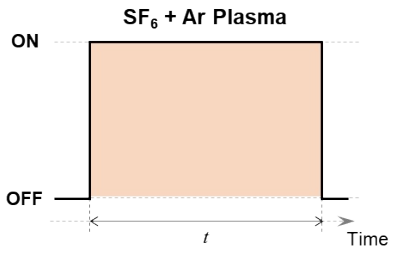	SF_6, 10 sccm + Ar, 100 sccm: 100 W, 3000 s Total etching time t = 3000 s	55.98 ± 0.04 Å / 60s

* This is the standard recipe used in the experiment.

Table S3. Comparison of different etching mechanisms.

#	Schematic	Parameters	EPC (Å/cyc)
3-1*	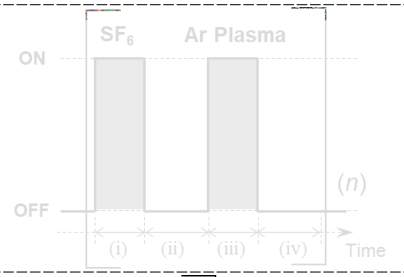	(v) SF_6, 20 sccm: 10 s (vi) Purge: 30 s (vii) Ar, 100 sccm: 100 W, 60 s (viii) Purge: 30 s Cycle number n = 50	1.38 ± 0.03
3-1	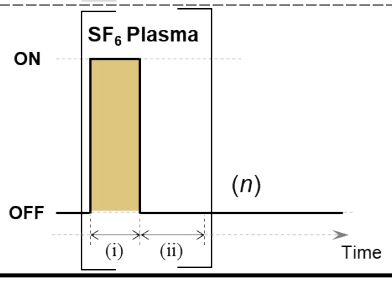	(i) SF_6, 20 sccm: 10 s, 100 W (ii) Purge: 30 s Cycle number n = 50	0.50 ± 0.03

* This is the standard recipe used in the experiment.

Figure caption for supporting videos:

Video S1. Adsorption of SF_6 molecules on a SiO_2 surface terminated with Si atoms.

Video S2. Adsorption of SF_6 molecules on a SiO_2 surface terminated with O atoms.